

Synthesis of Catalyst for Aqueous Polymerization: Perform Artificial Neural Network for the Prediction of Maximum Yield of Polymer

Deepal Agrawal¹, Nitish K Gupta¹, Yogesh Shrivastava^{2,*}

¹ Department of Applied Chemistry, Shri G. S. Institute of Technology and Science, Indore, M.P., India

² Department of Mechanical Engineering, Galgotias College of Engineering and Technology, Greater Noida, U.P., India

*Author to whom correspondence should be addressed:

E-mail: yogeshshrivastava90@gmail.com; yogesh.shrivastava@galgotiacollege.edu

(Received December 05, 2024; Revised July 22, 2025; Accepted August 02, 2025)

Abstract: This research synthesized a new catalyst $LTiCl_2$ using LH_2 , which is 2-(3, 5-Di-tert-butyl-2-hydroxybenzylamino)-succinic acid. This compound includes an additional donor to enhance the catalyst efficiency for the polymerization of polar olefins in aqueous medium. The properties of the resulting polymer were characterized by 1H NMR spectroscopy and dynamic light scattering (DLS). Moreover, it has been found that upon activation with BPh_4^- , the complex exhibits higher activity as a single-site catalytic species for polymerization reactions. These highly active species produce a syndiotactic-rich polymer with a narrow polydispersity index (PDI value in the range of 0.1-0.2). Moreover, the yield of the synthesized polymer has been measured at different combinations of catalyst, co-catalyst, and monomer. Furthermore, a prediction model has been developed to identify the variation in the yield of polymer concerning the variation in the moles of ingredients (catalyst, co-catalyst, and monomer). To develop the prediction model, an artificial neural network was employed. The analysis led to the identification of a safe zone that is predicted to achieve optimal yield. This zone was validated through additional experiments, and the results confirmed that it effectively maximizes polymer yield.

Keywords: early transition metal; Mathematical modeling; Non-metallocene catalyst; yield

1. Introduction

Today the field of post-metallocene catalytic systems based on titanium complexes for the production of ultra-high molecular weight polymers is overwhelmingly preferred¹⁻². The continuous evolution in the field of catalysts, and the discovery of FI catalysts by Fujita and co-workers hold an unrivaled place among those³. The copolymerization of ethylene with 5-hexene 1-yl acetate has been reported by Fujita³. This copolymerization reaction was catalyzed by a titanium-based bis(phenoxyiminate) complex⁴. With the valuable application and growing demand for polyolefins, researchers have focused on the synthesis of a metallocene catalyst⁵. Several researchers have synthesized the catalyst based on transition metal metallocene complex which upon activation with methylalumoxane (MAO) shows single-site catalytic behavior⁶⁻⁸.

Researchers have developed post-metallocene catalysts by modifying the properties of metallocene catalyst⁹. This post-metallocene catalyst is usually based on group 4-6

and 8-10 transition metals bearing multi-dentate organic ligand¹⁰⁻¹¹. Due to ligand-oriented structure, the complexes exhibit different geometry which is not shown by metallocene complex¹²⁻¹³. In 1990, the researchers reported post-metallocene complexes based on early transition metals i.e. phenoxy imine catalyst which bears salicylaldimine ligand¹⁴⁻¹⁵. This research has given a new idea to scientists for discovering high-activity catalysts¹⁶. Due to the large-scale production of olefin, there has been significant interest in developing post-metallocene catalysts¹⁷. In this regard, researchers have developed a range of catalytic systems which was based on post-metallocene catalysts. Indolide-imine, and pyrrolide-imine (PI), are examples of post-metallocene catalyst¹⁸⁻¹⁹. The design of ligand-oriented catalysts is particularly compelling because their performance is influenced by the electronic properties of the ligand. These catalysts are highly sensitive, and even small modifications in the ligand structure can significantly enhance catalytic activity and stereospecificity²⁰. The post-metallocene catalyst with

co-catalysts such as ion forming activator and methyl aluminoxane show high polymerization activity²¹⁻²²⁾

Water plays a vital role in organic synthesis concerning growing awareness of the need for a sustainable environment²³⁾. Most of the organic reactions are carried out in an organic solvent but these solvents have adverse effects on the environment. Although bio solvents are developed such as glycerol, bioethanol lignocellulosic biomass, etc. water holds a unique position among those²⁴⁾. The non-toxicity, non-inflammability, cost efficiency, environmental compatibility, and high heat capacity of water make it a widely recognized solvent²⁵⁾. To date, different polymerization reactions in aqueous medium have been studied. This reaction is based on a free radical-initiated mechanism. Recently, Spitz and Claverie et al. reported the synthesis of polyethylene. This reaction is catalyzed by an aqueous medium using nickel(II) as a catalyst²⁶⁻²⁷⁾.

In recent years, researchers have emphasized the importance of evaluating polymer yield to assess catalyst effectiveness. Numerous studies have focused on analyzing polymer quality. Some researchers have investigated the optimal ratio of catalyst, co-catalyst, and monomer to achieve maximum yield. Additionally, modeling techniques have been employed to assess catalyst quality. However, to the best of the authors' knowledge, there has been no significant research on using Artificial Neural Networks (ANN) to identify the optimal ratio of catalyst, co-catalyst, and monomer²⁸⁾. Several researchers have explored the application of Artificial Neural Networks (ANN) in chemical and polymer engineering to model complex, nonlinear systems. ANN has been effectively used to predict reaction kinetics, product distribution, and material properties in catalytic and polymerization processes. For instance, studies have demonstrated the utility of ANN in optimizing reaction conditions for polyethylene and polypropylene synthesis, as well as in modeling molecular weight distribution and melt flow index. In catalysis research, ANN has been employed to estimate catalyst activity, stability, and selectivity under varying operating conditions. These works highlight the capability of ANN to learn from limited experimental data and provide reliable predictions where traditional mathematical models may fall short. However, despite its growing use in polymer-related modeling, the application of ANN specifically for predicting the optimal ratio of catalyst, co-catalyst, and monomer in aqueous olefin polymerization remains underexplored, thereby underscoring the novelty of the present study.

The objective of this research work is to develop a newly designed catalyst with an extra donor atom for the polymerization reactions. We demonstrate that the catalytic activity can be enhanced by the side arm donor atom. To assess catalyst activity, polymer yield was

measured across 27 different combinations of catalyst, co-catalyst, and monomer. The experimental design was then used to train an Artificial Neural Network (ANN) to create a mathematical model for yield prediction. This model was analyzed to define a safe zone contour for the combinations. Further experiments were conducted to validate this safe zone. The results demonstrated that the identified zone is both relevant and significant. The synthesis process and characterization methods are reported in one of the author's published articles²⁹⁾. To achieve this goal, the research was guided by the following key objectives:

To synthesize and evaluate a novel [ONOO]-type catalyst with an additional donor atom aimed at enhancing polymerization activity.

To develop and train an Artificial Neural Network (ANN) model using experimental data to predict polymer yield and identify optimal reaction conditions.

To validate the ANN-predicted "safe zone" for catalyst, co-catalyst, and monomer ratios through targeted experiments.

2. Proposed methodology

For the simplified version of the proposed methodology, a flow chart was made in Figure 1. The underlying step is the synthesis of the ligand that will be used to make the catalyst. It is used in polymer production with this catalyst. It has been shown that the efficiency and effectiveness of a catalyst depend directly on polymer yield. 27 experiments were run to assess catalyst performance while varying the amounts of catalyst, co-catalyst, and MMA and measuring the amount of polymer yield. Artificial Neural Networks (ANN) were used to develop a mathematical model to determine optimal quantities of these components. The response variable yield (Y) was predicted using the input parameters, catalyst (C), co-catalyst (Co), and MMA (M)—to use the structure of the model. The model was validated and utilized to produce a safe zone contour, a shape of the input space that predicts which input parameters will yield the maximum. It provides a safe zone for the specification of the input values by which the highest polymer yield can be achieved most efficiently³⁰⁾.

3. Mathematical Modelling

Several mathematical modeling techniques are applicable to build the relationship between input and output parameters. This research uses Artificial Neural Networks (ANN) to achieve this objective³¹⁻³³⁾. Figure 2 shows the general ANN structure and Figure 3 shows the ANN structure used in this study. A structure was trained and tested to predict the yield of the polymer. The feedforward backpropagation learning method was used, i.e. when input values are fed into the network, propagated forward

through all layers, and subjected to a hidden layer. The input considered for the modeling is the catalyst (C), Co-catalyst, and MMA. The output considered is the yield. The Design of the experiment planned for ANN training and testing purposes is shown in Table 1.

4. ANN training and testing

In this study, the Artificial Neural Network (ANN) was trained and tested using a dataset of 27 experimental values, split in an 85:15 ratio. The ANN architecture has 3 input nodes, 2 hidden layers, and 1 output node. Three neurons (Catalyst, Co-catalyst, MMA) form the input layer. One is ten neurons in the first hidden layer and five neurons in the second hidden layer. The output layer has a single neuron Yield (Y). Thoughts from Heaton were used to select the number of hidden layers, and the methodology of Shrivastava et al. was implemented to learn the network³⁰⁻³⁴⁻³⁵.

The transfer function of the model used was the hyperbolic tangent, however Gaussian and Sigmoid were also tested.

R values were used to select the transfer function. The percentage error in predictions made by each model was compared to determine the most suitable transfer function. The predicted values from each transfer function were compared against the experimental output values and the percent errors were calculated as standard ANN testing, where *eai* represents average individual error, and *VE* and *VP* are experimental and predicted values, respectively. Moreover, from Table 1 it has been observed that the variation in the range of input parameters (C, Co, M) and output parameter (Y) is higher. Hence, the parameters have been normalized using the relations:

$$\text{Normalized } C = C/4 \tag{1}$$

$$\text{Normalized } Co = Co/4 \tag{2}$$

$$\text{Normalized } M = M/3.1 \tag{3}$$

$$\text{Normalized } Y = Y/3 \tag{4}$$

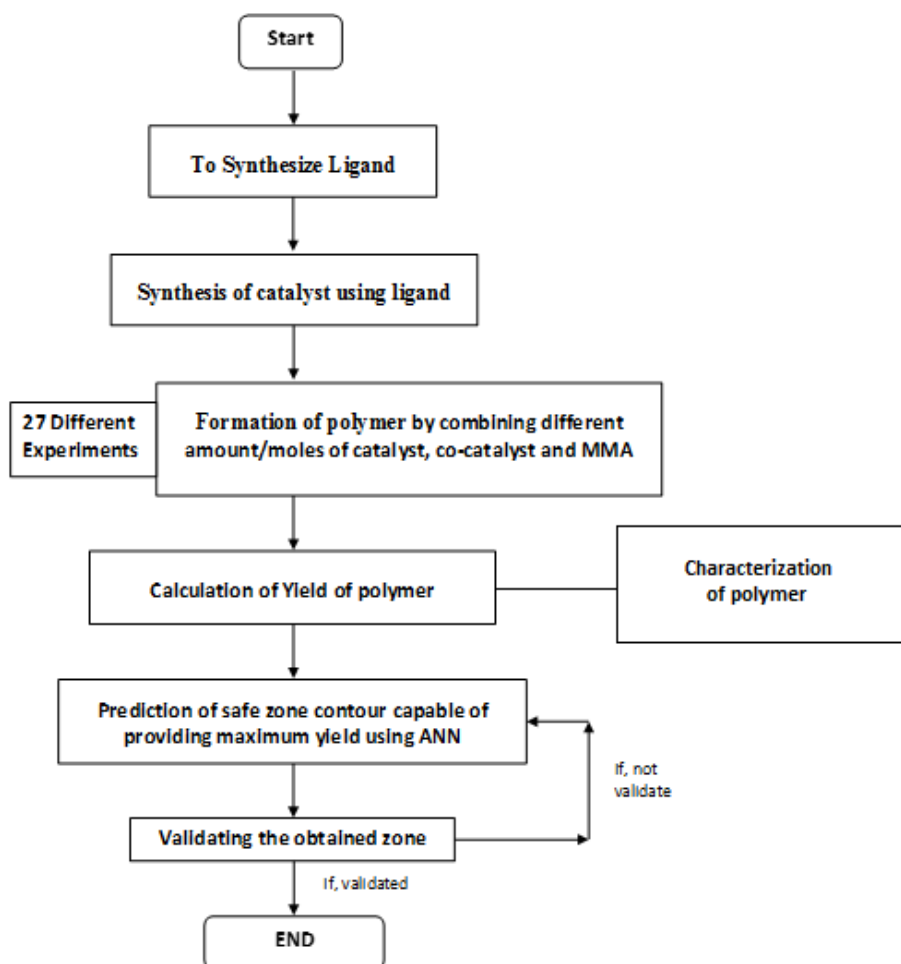


Fig. 1: Proposed methodology

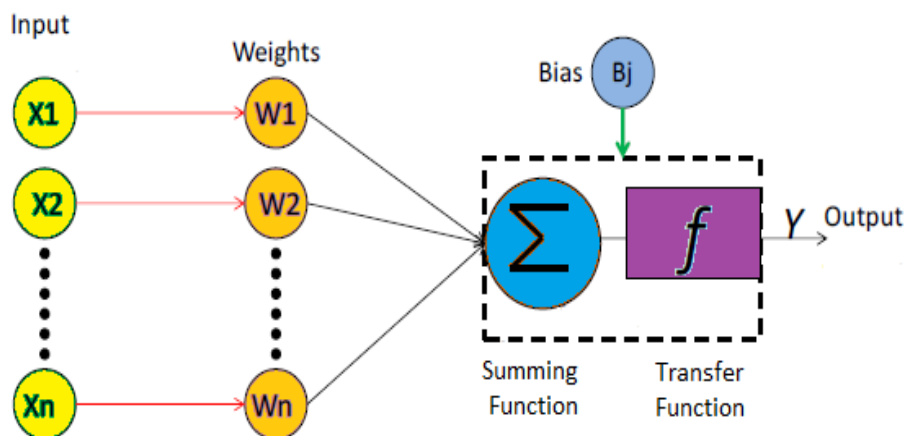


Fig. 2: The architecture of feed-forward back propagation ANN

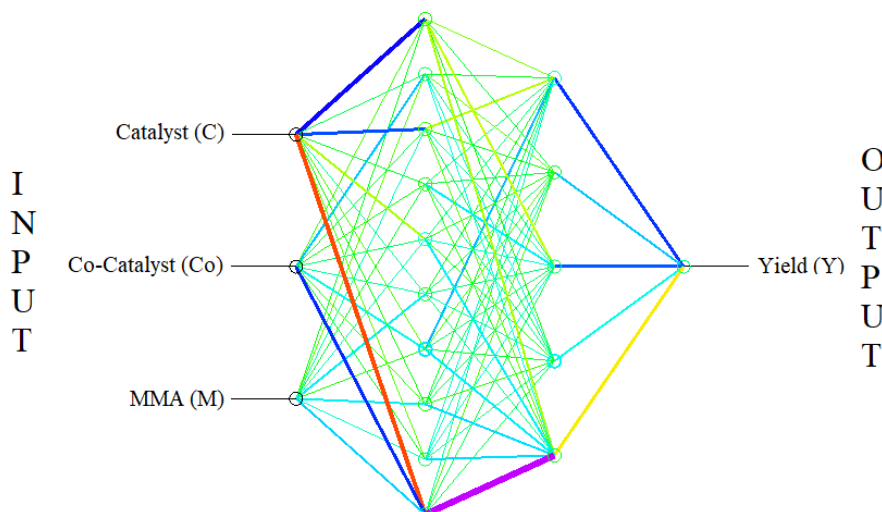


Fig. 3: Proposed ANN architecture

Table 1: Design of experiment and calculated yield

S.No.	C (mmol/L)	Co (mmol/L)	MMA (ml)	Y g (%)
1	1	1	2.1	0.97 (46.19)
2	1	1	2.6	0.93 (35.76)
3	1	1	3.1	0.89 (28.70)
4	1	2	2.1	1.2 (57.14)
5	1	2	2.6	0.99 (38.07)
6	1	2	3.1	0.96 (30.96)
7	1	4	2.1	1.1 (52.38)
8	1	4	2.6	1 (38.46)
9	1	4	3.1	0.91 (29.35)
10	2	1	2.1	1.21 (57.61)
11	2	1	2.6	1.99 (76.53)
12	2	1	3.1	1.95 (62.90)
13	2	2	2.1	1.74 (82.85)
14	2	2	2.6	1.71 (65.76)
15	2	2	3.1	1.68 (54.19)
16	2	4	2.1	1.77 (84.28)
17	2	4	2.6	1.74 (66.925)
18	2	4	3.1	1.75 (56.45)
19	4	1	2.1	0.51 (24.28)
20	4	1	2.6	0.47 (18.07)

21	4	1	3.1	0.44 (14.19)
22	4	2	2.1	0.61 (29.04)
23	4	2	2.6	0.59 (22.69)
24	4	2	3.1	0.56 (18.06)
25	4	4	2.1	1.84 (87.61)
26	4	4	2.6	1.82 (70)
27	4	4	3.1	1.79 (57.74)

Table 2: Connection weights between input and first hidden layer

Neurons	W_{Dk}	W_{Sk}	W_{Fk}	B_{1k}
A	-1.4695	-2.5394	0.69975	3.0162
B	2.1763	0.58234	-2.0056	-2.3459
C	2.5645	-0.30937	1.5573	-1.6757
D	-0.67155	-2.7417	1.0628	1.0054
E	0.67185	-1.6135	2.4582	-0.33513
F	-2.3496	-1.8714	-0.27398	-0.33513
G	-1.9863	1.3105	-1.8533	-1.0054
h	0.28003	-1.7165	-2.4643	1.6757
i	1.6854	0.17226	2.4954	2.3459
j	2.0175	-1.5543	-1.616	3.0162

Where, W_{Dk} , W_{Sk} , and W_{Fk} indicate weights between input and first hidden layer, B_{1k} is the bias for layer one and k varies from a to j neurons.

Table 3: The connection weights between the first hidden layer and the second hidden layer

Neurons	W_{ak}	W_{bk}	W_{ck}	W_{dk}	W_{ek}	W_{fk}	W_{gk}	W_{hk}	W_{ik}	W_{jk}	B_{hk}
P	0.55742	-0.67296	0.63078	-0.11734	-0.62263	0.60398	-0.72546	-0.14154	-0.01839	0.47947	0.55742
Q	0.06254	0.75344	-0.67786	0.66984	0.60238	0.19909	-0.42424	-0.73459	-0.26471	-0.17985	0.062543
R	0.7568	-0.75563	-0.15287	-0.48531	0.12158	-0.22736	-0.57459	0.6143	0.61024	-0.39402	0.7568
S	-0.83286	0.54279	-0.47412	-0.46635	0.098445	0.02616	-0.6241	0.87819	-0.25816	-0.18972	-0.83286
T	-0.10303	0.57032	0.53934	-0.63711	-0.63816	-0.17649	-0.46741	-0.01642	-0.69882	-0.72533	-0.10303

Where, w_{ak}, \dots, w_{ik} , and w_{jk} indicate the weights between the first and second hidden layer, B_{hk} is the bias for layer two, and k varies from p to t .

Table 4: The connection weights between the hidden layer and the output layer

Neuron	W_{po}	W_{qo}	W_{ro}	W_{so}	W_{to}	B_o
O	-0.59962	-0.59962	0.72022	0.74317	0.12254	0.00076

$$e_{ai} = \left(\frac{V_E - V_P}{V_E} \right) \times 100\% \quad (5)$$

5. The mathematical expression for the ANN

The mathematical model for the output was developed using the weights assigned to each transition: from the input layer to the first hidden layer, from the first hidden layer to the second hidden layer, and from the second hidden layer to the output. The weights obtained for these transitions are detailed in Tables 2 to 4.

Now, for calculating “ O ” the following expression can be used;

$$O = w_{po} \times p + w_{qo} \times q + w_{ro} \times r + w_{so} \times s + w_{to} \times t + B_o \quad (6)$$

where, w_{po}, \dots, w_{so} , and w_{to} indicate the weights between the second and output hidden layer, and B_o is the bias for

layer three.

Y has been obtained as;

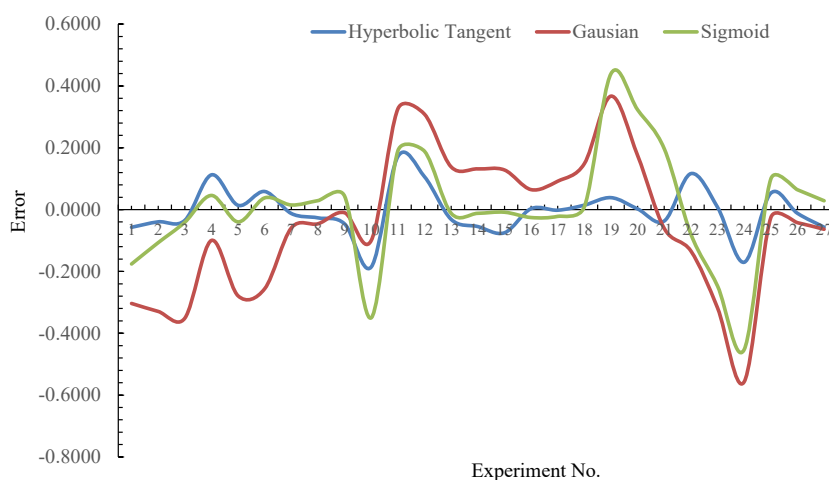
$$y(Y) = \frac{2}{[1 + \exp(-2 \times O)]} - 1 \quad (7)$$

Results and discussion

Yield prediction was performed using a backpropagation neural network with three different transfer functions. A comparative analysis was conducted to determine the most suitable transfer function for prediction. This evaluation was based on comparisons of R-values for the training and testing sets, as well as the percentage error between predicted and experimental values.

5.1. Comparison between different transfer functions

Yield is then evaluated and the ANN architecture was then built, the details of which are listed in Table 5 for training and testing purposes. Various training-to-testing ratios


Fig. 4: Comparison between different transfer functions

have been suggested by researchers, such as 90:10%, 85:15%, and 80:20%. For this study, a ratio of 85:We chose 15 %, that is 27 experimental samples, 23 for training, and 4 for testing.

These were not the data used during ANN training. Hyperbolic tangent, Gaussian, and sigmoid were sequentially applied during training as three transfer functions. Table 5 presents the predicted values and associated errors. Results show that the hyperbolic tangent function provides the lowest average error (0.4224) to 1.359 for a Gaussian function and 0.7574 for a sigmoid function. Figure 4 also illustrates these findings. Table 6 lists the R values for the three transfer functions, and Figures 5-7 give the regression plots for the three transfers.

The regression plot indicates that the hyperbolic tangent transfer function is the most suitable for yield analysis. The corresponding R-values are 0.957 for training and 0.946 for testing. Figure 8 illustrates the plot of actual versus predicted yield values when using the hyperbolic tangent transfer function in the ANN.

5.2. Safe zone prediction based on ANN

Results from the hyperbolic tangent transfer function-based ANN were analyzed to obtain the safe zone contour. Contour plots were produced for various combinations of the input parameters to better visualize the optimal region of these parameters for maximum yield, with yield as the output.

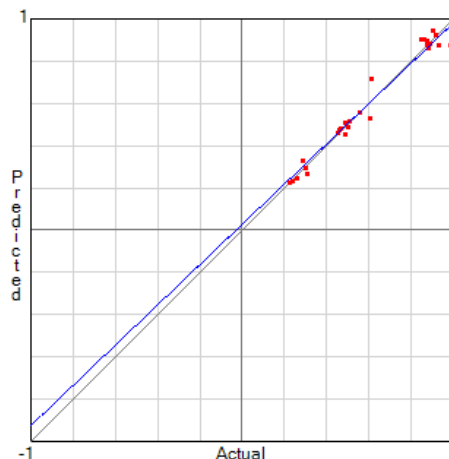


Figure 5: Hyperbolic tangent transfer function

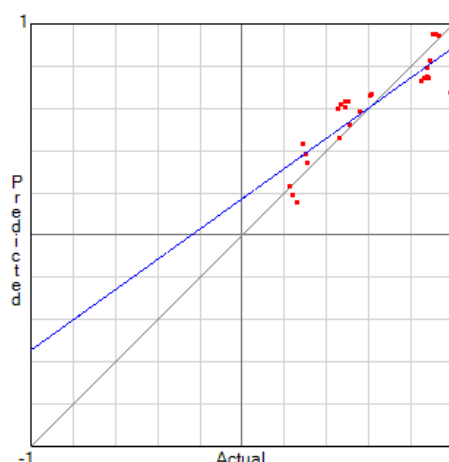


Fig. 6: Gaussian transfer function

Table 5: Comparison of three activation functions (Values in Normalized form)

(C)	(Co)	(M)	Exp. Y	Pred. Y Hyperbolic tangent (HT)	Error (HT)	Pred. Y Gaussian (G)	Error (G)	Pred. Y Sigmoid (S)	Error (S)
0.25	0.25	0.677	0.366	0.515	-0.0571	0.635	-0.3036	0.573	-0.1759
0.25	0.25	0.838	0.333	0.485	-0.0396	0.621	-0.3294	0.517	-0.1069
0.25	0.25	1	0.303	0.462	-0.0349	0.604	-0.3513	0.465	-0.0408
0.25	0.5	0.677	0.403	0.535	0.1125	0.663	-0.0996	0.575	0.0458
0.25	0.5	0.838	0.663	0.490	0.0139	0.636	-0.2790	0.517	-0.0397
0.25	0.5	1	0.650	0.454	0.0586	0.605	-0.2558	0.464	0.0380
0.25	1	0.677	0.580	0.559	-0.0127	0.585	-0.0591	0.544	0.0150
0.25	1	0.838	0.570	0.515	-0.0267	0.525	-0.0458	0.487	0.0291
0.25	1	1	0.560	0.478	-0.0463	0.461	-0.0102	0.437	0.0433
0.5	0.25	0.677	0.590	0.720	-0.1854	0.668	-0.0996	0.820	-0.3499
0.5	0.25	0.838	0.580	0.828	0.1718	0.673	0.3260	0.809	0.1903
0.5	0.25	1	0.583	0.875	0.1062	0.677	0.3085	0.795	0.1886
0.5	0.5	0.677	0.170	0.901	-0.0316	0.753	0.1382	0.884	-0.0119
0.5	0.5	0.838	0.156	0.906	-0.0548	0.746	0.1317	0.869	-0.0120
0.5	0.5	1	0.146	0.907	-0.0750	0.736	0.1282	0.851	-0.0084

Cite: D. Agrawal, N.K. Gupta, Y. Shrivastava, "Synthesis of Catalyst for Aqueous Polymerization: Perform Artificial Neural Network for The Prediction of Maximum Yield of Polymer". Evergreen, 12 (03) 1520-1530 (2025). <https://doi.org/10.5109/7388846>.

0.5	1	0.677	0.203	0.886	0.0031	0.831	0.0646	0.912	-0.0256
0.5	1	0.838	0.196	0.876	-0.0019	0.794	0.0919	0.893	-0.0218
0.5	1	1	0.186	0.866	0.0144	0.748	0.1486	0.871	0.0091
1	0.25	0.677	0.613	0.246	0.0387	0.162	0.3671	0.143	0.4397
1	0.25	0.838	0.606	0.235	0.0021	0.194	0.1748	0.159	0.3228
1	0.25	1	0.596	0.229	-0.0367	0.234	-0.0610	0.177	0.1968
1	0.5	0.677	0.366	0.270	0.1165	0.347	-0.1340	0.330	-0.0795
1	0.5	0.838	0.333	0.294	0.0076	0.390	-0.3180	0.369	-0.2472
1	0.5	1	0.303	0.329	-0.1703	0.438	-0.5570	0.408	-0.4527
1	1	0.677	0.403	0.875	0.0533	0.948	-0.0259	0.833	0.0991
1	1	0.838	0.663	0.925	-0.0119	0.953	-0.0423	0.855	0.0642
1	1	1	0.650	0.950	-0.0569	0.956	-0.0636	0.873	0.0286
Average Error					0.4224	1.359996		0.757426	

Table 6: R – Values

R-Value	Hyperbolic Tangent	Gaussian	Sigmoid
Training	0.957	0.767	0.899
Testing	0.946	0.699	0.891

In Figs. 9–11, these plots were drawn by varying two input parameters at a time. Areas of maximum yield, which are denoted by red, can be seen in these Figures. Figure 9 (C-Co Contour): At normalized values of Co > 0.5 and Co > 0.5, the yield is maximized. Based on this, higher moles of the co-catalyst with relatively lesser moles of catalyst lead to better yield. Figure 10 (C-M Contour): At higher amounts of the catalyst and MMA, maximum yield is obtained. The expected optimum value of the normalized catalyst is 0.4. Figure 11 (Co-M Contour): Co is nearly independent of the yield and M > 0.5 gives a better yield. These contour plots help us understand what the relationships are between the input parameters and give us an idea of the optimal parameters to have for maximum polymer yield.

A three-parameter contour plot was generated to identify the combined effect of all three parameters on yield, as shown in Figure 12. In particular, this Figure shows a safe zone contour. Based on the contour, maximum yield can be realized within the safe zone when Catalyst (C) is normalized at 0.25, Co-catalyst (Co) is between 0.13 and 0.5, and Monomer (M) is greater than 0.2 normalized.

To further validate the identified range, additional experiments were conducted using a design of experiment based on the established safe zone. Table 7 presents the various combinations of input parameters and the corresponding yield (Y) obtained from these experiments. From the validation results, it is clear that the obtained safe zone contour is valid as the values of experimentally calculated yield and predicted yield are very close. Moreover, maximum yield i.e. 2.41 has been obtained at which the percentage of yield is 93.05 %. The proposed

methodology can be used by researchers to approximate the amount/ moles of complexes viz. (co-catalyst, catalyst, etc.) that may result in maximum yield.

The comparative analysis of three transfer functions demonstrated that the hyperbolic tangent function offered the best prediction accuracy, with the lowest average error and highest R-values (0.957 for training and 0.946 for testing). This function was thus selected to develop a reliable ANN model for polymer yield prediction. Contour plots derived from the trained model revealed clear trends among the input parameters, allowing the identification of a “safe zone” where polymer yield is maximized. Experimental validation within this zone confirmed the model’s predictive strength, with the maximum observed yield reaching 93.05%. These results establish the ANN-based approach as a powerful and practical tool for

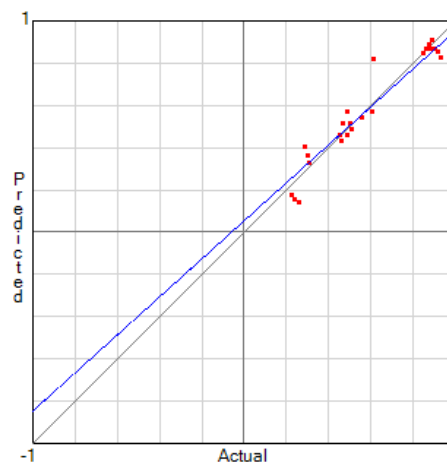


Fig. 7: Sigmoid transfer function

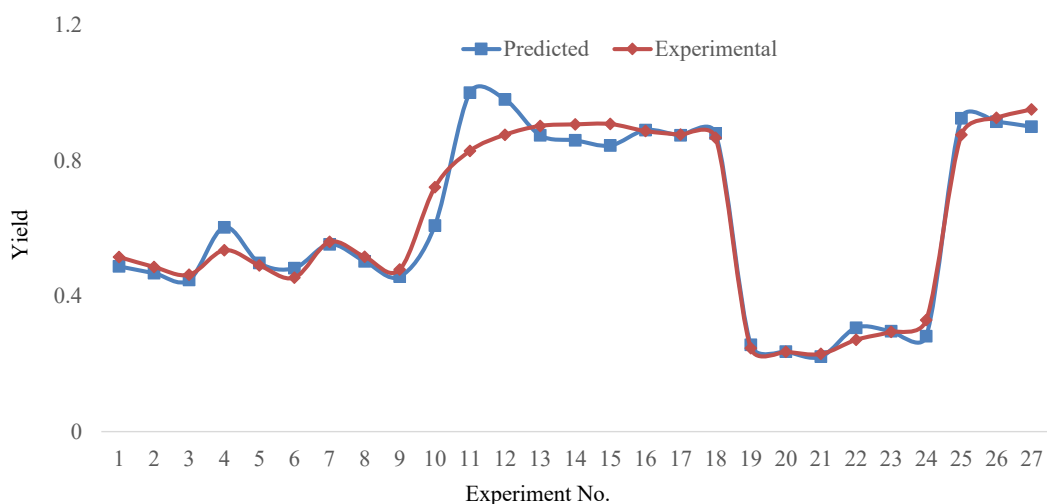


Fig. 8: Experimental vs predicted values

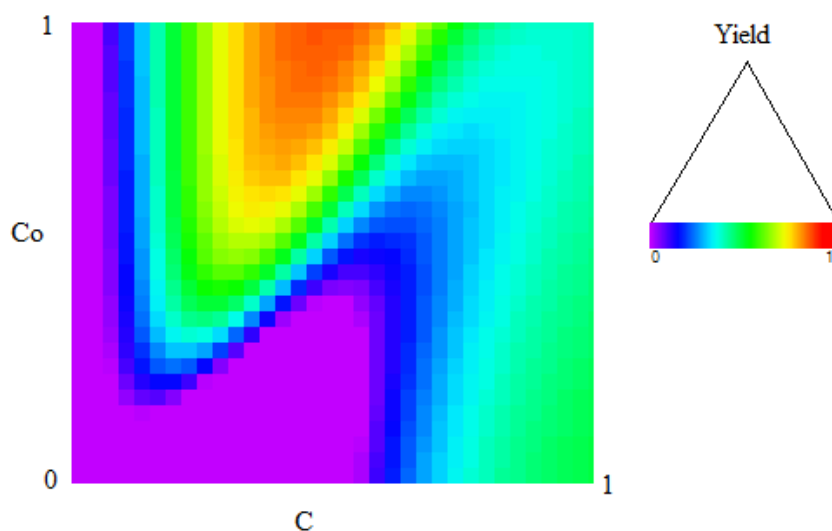


Fig. 9: Contour plot between normalized C and Co

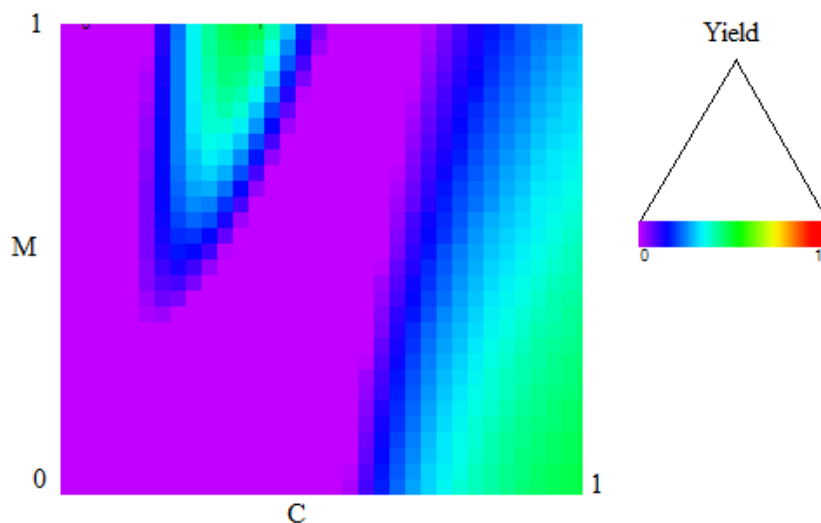


Fig. 10: Contour plot between normalized C and M

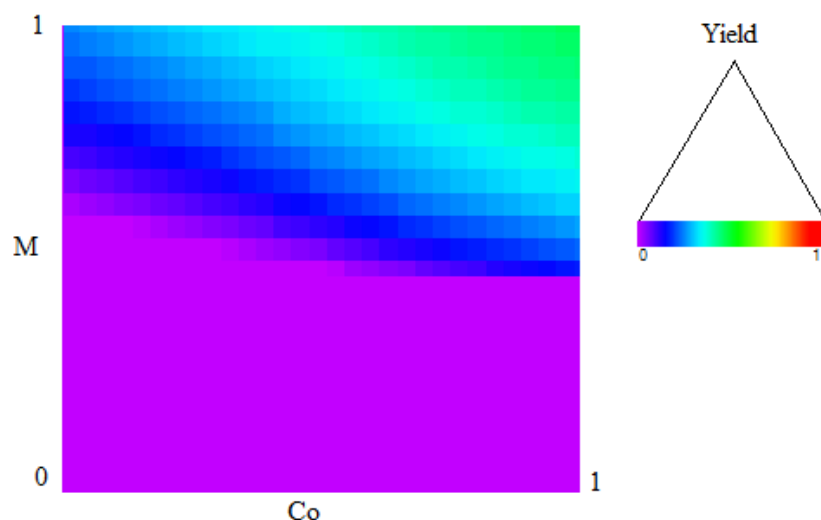


Fig. 11: Contour plot between normalized Co and M

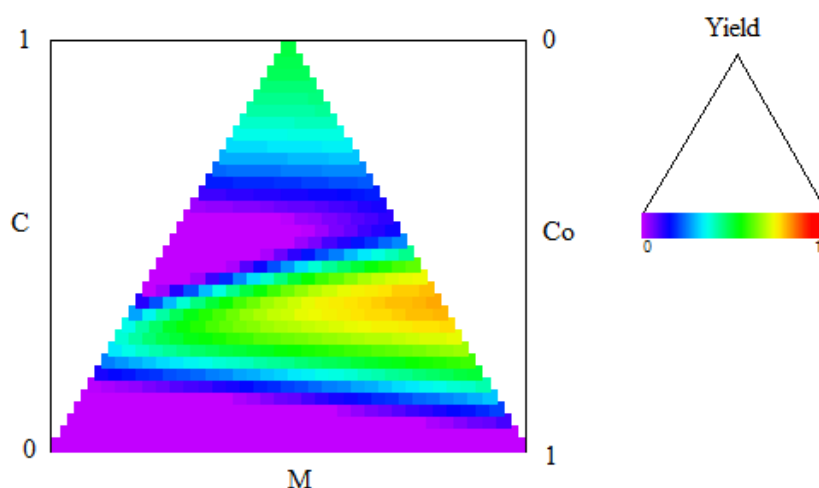


Fig. 12: Contour between normalized C, Co, and M

Table 7: Combination of input parameters and obtained yield

S. no.	Normalized C	Actual C	Normalized Co	Actual Co	Normalized M	Actual M	Predicted Y	Experimental Y
1	0.3	1.2	0.35	1.4	0.9	2.59	2.44	2.41 (93.05%)
2	0.2	0.8	0.25	1	0.6	1.86	1.39	1.36 (73.11%)
3	0.5	2	0.5	2	0.5	1.55	0.58	0.55 (37.41%)

optimizing catalyst, co-catalyst, and monomer ratios to achieve efficient polymerization with minimal trial-and-error experimentation.

6. Conclusion

The synthesis of an asymmetric [ONOO]-type tetradentate ligand was achieved, and its catalytic activity was evaluated for olefin polymerization in an aqueous medium at room temperature. This study focused on optimizing polymer yield through both experimental investigation and predictive modeling using Artificial Neural Networks

(ANN). A total of 27 experimental combinations were systematically explored by varying the amounts of catalyst, co-catalyst, and monomer to analyze their effect on polymer yield. The ANN model was then employed to identify the optimal input conditions for maximum yield. Based on model predictions, a “safe zone” was established—an optimal range of catalyst, co-catalyst, and monomer concentrations that consistently yielded high polymer output. This safe zone was further validated through additional experiments, confirming its reliability. The maximum polymer yield achieved during the study was 93.05%. This integrated experimental and ANN-based

approach provides a robust framework for researchers to efficiently determine ideal reactant proportions, enabling high-yield, room-temperature polymerization in aqueous systems.

References

- 1) C. Wang et al., "Novel titanium catalysts bearing an [O, N, S] tridentate ligand for ethylene homo- and copolymerization," *Macromol. Rapid Commun.*, vol. 26, no. 20, pp. 1609–1614, 2005. DOI: 10.1002/marc.200500403
- 2) R. Gauvin, A. Arbaoui, E. Gautier, A. Mortreux, E. Berrier, and G. J. A. Nowogrocki, "Efficient synthesis and structural characterization of a post-metallocene α -olefin polymerization catalyst," *Inorg. Chim. Acta*, vol. 362, no. 1, pp. 277–280, 2009. DOI: 10.1016/j.ica.2008.02.034
- 3) T. Fujita and K. Kawai, "FI catalysts for olefin oligomerization and polymerization: Production of useful olefin-based materials by unique catalysis," *Top. Catal.*, vol. 57, no. 10–13, pp. 852–877, 2014. DOI: 10.1007/s11244-014-0246-z
- 4) A. Ishii, K. Ikuma, N. Nakata, K. Nakamura, H. Kuribayashi, and K. Takaoki, "Zirconium and hafnium complexes with cycloheptane- or cyclononane-fused [OSSO]-type bis(phenolato) ligands: Synthesis, structure, and highly active 1-hexene polymerization," *Organometallics*, vol. 36, no. 20, pp. 3954–3966, 2017. DOI: 10.1021/acs.organomet.7b00586
- 5) W. Kaminsky, A. Funck, and H. Hähnsen, "New application for metallocene catalysts in olefin polymerization," *Dalton Trans.*, no. 41, pp. 8803–8810, 2009. DOI: 10.1039/B910542P
- 6) E. L. Marshall and V. C. Gibson, "Stereoselective acrylate polymerization," in *Stereoselective Polymerization with Single-Site Catalysts*, CRC Press, 2007, pp. 611–644. DOI: 10.1201/9781420017083
- 7) M. R. Prabowo, A. P. Rachmadian, N. F. Ghazalli, and H. O. Lintang, "Chemosensor of gold(I) 4-(3,5-dimethoxybenzyl)-3,5-dimethyl pyrazolate complex for quantification of ethanol in aqueous solution," *Evergreen*, vol. 7, no. 3, pp. 404–408, 2020. DOI: 10.5109/4068620
- 8) E. R. Dyartanti, I. N. Widiassa, A. Purwanto, and H. Susanto, "Nanocomposite polymer electrolytes in PVDF/ZnO membranes modified with PVP for LiFePO₄ batteries," *Evergreen*, vol. 5, no. 2, pp. 19–25, 2018. DOI: 10.5109/1936213
- 9) A. A. Antonov and K. P. Bryliakov, "Post-metallocene catalysts for the synthesis of ultrahigh molecular weight polyethylene: Recent advances," *Eur. Polym. J.*, vol. 142, p. 110162, 2021. DOI: 10.1016/j.eurpolymj.2020.110162
- 10) G. P. Goryunov et al., "Rigid postmetallocene catalysts for propylene polymerization: Ligand design prevents the temperature-dependent loss of stereo- and regioselectivities," *ACS Catal.*, vol. 11, no. 13, pp. 8079–8086, 2021. DOI: 10.1021/acscatal.1c01611
- 11) K. Sharma, S. K. De, and P. Singh, "A post-metallocene titanium(IV) complex bearing asymmetric tetradentate [ONNO]-type amino acid-based ligand and its activity toward polymerization of polar monomers in aqueous emulsion," *Colloid Polym. Sci.*, vol. 294, no. 12, pp. 2051–2070, 2016. DOI: 10.1007/s00396-016-3970-z
- 12) C.-C. Liu, Q. Liu, S.-M. Yiu, and M. C. Chan, "Group 4 post-metallocenes supported by [OCH₂N, C(σ -aryl)] auxiliaries bearing a seven-membered metallacycle: Synthesis, characterization, and catalysts for olefin polymerization," *Organometallics*, vol. 38, no. 15, pp. 2963–2971, 2019. DOI: 10.1021/acs.organomet.9b00307
- 13) A. Pärssinen, P. Elo, M. Klinga, M. Leskelä, and T. Repo, "Synthesis of titanium complexes bearing malonic acid ester ligands and their use as catalyst precursors in ethene polymerization," *Inorg. Chem. Commun.*, vol. 9, no. 8, pp. 859–861, 2006. DOI: 10.1016/j.inoche.2006.05.006
- 14) L. de Oliveira, S. da Silva, A. Casagrande, R. Stieler, and O. A. C. Casagrande Jr, "Synthesis and characterization of Ni(II) complexes supported by phenoxy/naphthoxy-imine ligands with N- and O-donor groups for ethylene oligomerization," *Appl. Organomet. Chem.*, vol. 32, no. 7, p. e4414, 2018. DOI: 10.1002/aoc.4414
- 15) Y. Suzuki, H. Tanaka, T. Oshiki, K. Takai, and T. Fujita, "Titanium and zirconium complexes with non-salicylaldimine-type imine-phenoxy chelate ligands: Syntheses, structures, and ethylene-polymerization behavior," *Chem. Asian J.*, vol. 1, no. 6, pp. 878–887, 2006. DOI: 10.1002/asia.200600256
- 16) S. Kudo, K. Norinaga, and J.-i. Hayashi, "Applications of catalysis in the selective conversion of lignocellulosic biomass by pyrolysis," *Kyushu Univ. Institutional Repository*, 2012. DOI: <http://hdl.net/2324/25216>
- 17) D. Agrawal, S. K. De, and P. Singh, "Synthesis and characterization of post-metallocene titanium complexes of bidentate dicarboxylic acids: Effect of ring size on polymerization in aqueous emulsion," *J. Polym. Res.*, vol. 27, pp. 1–9, 2020. DOI: 10.1007/s10965-020-02067-8
- 18) V. C. Gibson, C. Redshaw, and G. A. Solan, "Bis(imino)pyridines: surprisingly reactive ligands and a gateway to new families of catalysts," *Chem.*

- Rev., vol. 107, no. 5, pp. 1745–1776, 2007. DOI: 10.1021/cr068437y
- 19) M. Tanabiki, K. Matsubara, Y. Sunada, and H. Nagashima, "Catalyst design of novel nickellacyclic complexes for ethylene polymerization," *Catal. Commun.*, vol. 11, pp. 16–23, 2010.
 - 20) T. Gueta-Neyroud, B. Tumanskii, M. Botoshansky, and M. S. Eisen, "Synthesis, characterization and catalytic activity of titanium bis(dimethylmalonate)–bis(diethylamido) complexes in propylene polymerization," *J. Organomet. Chem.*, vol. 692, no. 5, pp. 927–939, 2007. DOI: 10.1016/j.jorganchem.2006.10.03.doi.org/10.1016/j.jorganchem.2006.10.031
 - 21) M. C. Baier, M. A. Zuideveld, and S. Mecking, "Post-metallocenes in the industrial production of polyolefins," *Angew. Chem. Int. Ed.*, vol. 53, no. 37, pp. 9722–9744, 2014. DOI: 10.1002/anie.201400799
 - 22) Y. Suzuki et al., "Trimerization of ethylene to 1-hexene with titanium complexes bearing phenoxy–imine ligands with pendant donors combined with MAO," *Organometallics*, vol. 29, no. 11, pp. 2394–2396, 2010. DOI: 10.1021/om1003368
 - 23) M.-O. Simon and C.-J. Li, "Green chemistry oriented organic synthesis in water," *Chem. Soc. Rev.*, vol. 41, no. 4, pp. 1415–1427, 2012. DOI: 10.1039/C1CS15222J
 - 24) A. Berkefeld and S. Mecking, "Mechanistic studies of catalytic polyethylene chain growth in the presence of water," *Angew. Chem. Int. Ed.*, vol. 45, no. 36, pp. 6044–6046, 2006. DOI: 10.1002/anie.200601387
 - 25) S. Mecking and P. De, "Polymer dispersions from catalytic polymerization in aqueous systems," *Colloid Polym. Sci.*, vol. 285, no. 6, pp. 605–619, 2007. DOI: 10.1007/s00396-006-1587-3
 - 26) F. M. Bauers, M. M. Chowdhry, and S. Mecking, "Catalytic polymerization of ethylene in aqueous emulsion with a simple in situ catalyst," *Macromolecules*, vol. 36, no. 18, pp. 6711–6715, 2003. DOI: 10.1021/ma034164m
 - 27) J. Huber and S. Mecking, "Aqueous poly(arylacetylene) dispersions," *Macromolecules*, vol. 43, no. 21, pp. 8718–8723, 2010. DOI: 10.1021/ma1013572
 - 28) A. Sethi, A. Sharma, S. Chandra, and A. Rawat, "The photovoltaic (PV) module performance analysis using artificial neural network (ANN)," *Evergreen*, 2024. DOI: 10.5109/7183435
 - 29) D. Agrawal, Y. Shrivastava, S. De, and P. Singh, "Synthesis of post-metallocene catalyst and study of its olefin polymerization activity at room temperature in aqueous solution followed by prediction of yield," *J. Polym. Res.*, vol. 26, no. 7, p. 167, 2019. DOI: 10.1007/s10965-019-1825-2
 - 30) Y. Shrivastava and B. Singh, "Application of EEMD in determining tool chatter behavior using ANN approach," in *Proc. 10th Int. Conf. Precision Meso, Micro and Nano Engineering*, Dec. 07–10, 2017.
 - 31) Y. Shrivastava, B. Singh, and A. Sharma, "Analysis of tool chatter in terms of chatter index and severity using a new adaptive signal processing technique," *Exp. Tech.*, vol. 42, no. 2, pp. 141–153, 2018. DOI: 10.1007/s40799-017-0208-z
 - 32) A. Li, A. B. Ismail, K. Thu, M. W. Shahzad, K. C. Ng, and B. B. Saha, "Formulation of water equilibrium uptakes on silica gel and ferroaluminophosphate zeolite for adsorption cooling and desalination applications," *Evergreen*, vol. 1, no. 2, pp. 37–45, 2014. DOI: 10.5109/1495162
 - 33) S. R. Dixit, S. R. Das, and D. Dhupal, "Parametric optimization of Nd:YAG laser microgrooving on aluminum oxide using integrated RSM-ANN-GA approach," *J. Ind. Eng. Int.*, vol. 15, no. 2, pp. 333–349, 2019. DOI: 10.1007/s40092-018-0295-1
 - 34) Y. Shrivastava and B. Singh, "Possible way to diminish the effect of chatter in CNC turning based on EMD and ANN approaches," *Arab. J. Sci. Eng.*, vol. 43, no. 9, pp. 4571–4591, Nov. 30, 2017. DOI: 10.1007/s13369-017-2993-1
 - 35) H. R. Hafizpour, M. Sanjari, and A. Simchi, "Analysis of the effect of reinforcement particles on the compressibility of Al–SiC composite powders using a neural network model," *Mater. Des.*, vol. 30, no. 5, pp. 1518–1523, 2009. DOI: 10.1016/j.matdes.2008.07.052.